AEM
Journals.ASM.org

Isotope-Assisted Screening for Iron-Containing Metabolites Reveals a High Degree of Diversity among Known and Unknown Siderophores Produced by *Trichoderma* spp.

Sylvia M. Lehner,[a] Lea Atanasova,[b] Nora K. N. Neumann,[a] Rudolf Krska,[a] Marc Lemmens,[c] Irina S. Druzhinina,[b] Rainer Schuhmacher[a]

Center for Analytical Chemistry, Department for Agrobiotechnology (IFA-Tulln), University of Natural Resources and Life Sciences (BOKU), Vienna, Austria[a]; Research Group Microbiology, Institute of Chemical Engineering, Vienna University of Technology, Vienna, Austria[b]; Institute for Biotechnology in Plant Production, Department for Agrobiotechnology (IFA-Tulln), University of Natural Resources and Life Sciences (BOKU), Vienna, Austria[c]

Due to low iron availability under environmental conditions, many microorganisms excrete iron-chelating agents (siderophores) to cover their iron demands. A novel screening approach for the detection of siderophores using liquid chromatography coupled to high-resolution tandem mass spectrometry was developed to study the production of extracellular siderophores of 10 wild-type *Trichoderma* strains. For annotation of siderophores, an in-house library comprising 422 known microbial siderophores was established. After 96 h of cultivation, 18 different iron chelators were detected. Four of those (dimerum acid, fusigen, coprogen, and ferricrocin) were identified by measuring authentic standards. *cis*-Fusarinine, fusarinine A and B, and des-diseryl-glycylferrirhodin were annotated based on high-accuracy mass spectral analysis. In total, at least 10 novel iron-containing metabolites of the hydroxamate type were found. On average *Trichoderma* spp. produced 12 to 14 siderophores, with 6 common to all species tested. The highest number (15) of siderophores was detected for the most common environmental opportunistic and strongly fungicidic species, *Trichoderma harzianum*, which, however, did not have any unique compounds. The tropical species *T. reesei* had the most distinctive pattern, producing one unique siderophore (*cis*-fusarinine) and three others that were present only in *T. harzianum* and not in other species. The diversity of siderophores did not directly correlate with the antifungal potential of the species tested. Our data suggest that the high diversity of siderophores produced by *Trichoderma* spp. might be the result of further modifications of the nonribosomal peptide synthetase (NRPS) products and not due to diverse NRPS-encoding genes.

Iron is the fourth most abundant element in earth's crust (1). It is an essential trace mineral required for a healthy diet by almost all organisms and is involved in electron transport in metabolic processes, such as respiration and photosynthesis (2). Despite its abundance in nature, the amount of bioavailable iron is limited, as atmospheric oxygen rapidly oxidizes iron to ferric oxyhydroxides (3) that are poorly soluble under neutral to alkaline pH (4). In the case of fungi, the minimum iron requirement for optimal growth was reported to be 10^{-5} to 10^{-7} M (corresponding to approximately 6 to 600 μg/liter) (5). One strategy of plants and microbes for accessing iron is the production and excretion of siderophores. Siderophores (from the Greek sideros, "iron," and phorein, "to carry something") are ferric-iron-chelating, low-molecular-mass compounds (500 to 1,500 Da) (6) that are produced under iron depletion (7). Microbial siderophores show a very high binding constant for iron ($>10^{30}$ M, depending on the pH), enabling them to extract iron even from stainless steel (8).

Interestingly, it has been shown that monohydroxamate and dihydroxamate siderophores of fungal origin increase iron uptake by plants. It was suggested that (hydrolysis products of) fungal siderophores can play an important role in increasing iron availability for plants in soils with small amounts of accessible iron (9). Most fungal siderophores belong to the group of hydroxamate siderophores. Hydroxamate siderophores share the structural unit N^5-acyl-N^5-hydroxyornithine (2) and can be divided into three distinct groups: fusarinines, coprogens, and ferrichromes. They differ in the types of building blocks (N^5-acyl groups or amino acids) and how these building blocks are connected (ester/peptide bonds and/or head-to-head or head-to-tail order) (2, 10). Most of the fungal siderophores contain three hydroxamate groups and form hexadentate octahedral complexes with Fe^{3+} (6). Moreover, they are usually synthesized with the aid of nonribosomal peptide synthetases (NRPSs) and are mostly derived from L-ornithine (2). The first step in the biosynthetic pathway is hydroxylation of L-ornithine by ornithine-N^5-monooxygenases to N^5-hydroxy-L-ornithine. Second, the hydroxamate group is formed by transfer of an acyl group from acyl-coenzyme A (CoA) derivatives to N^5-hydroxyornithine. This results in N^5-acyl-N^5-hydroxy-L-ornithine with different possible acyl groups (Fig. 1). In a third step, NRPSs covalently link these units via ester or peptide bonds to linear or cyclic oligomeric iron chelators. Last, the NRPS products can be further modified by non-NRPS enzymes to yield a diversity of different siderophores originating from a single NRPS (8).

Many species of the filamentous mycotrophic fungus *Trichoderma* (teleomorph *Hypocrea*, Ascomycota, Dikarya) can be used

Received 26 July 2012 Accepted 28 September 2012
Published ahead of print 12 October 2012
Address correspondence to Rainer Schuhmacher, rainer.schuhmacher@boku.ac.at.
L.A. and N.K.N.N. contributed equally to the research.
Supplemental material for this article may be found at http://dx.doi.org/10.1128/AEM.02339-12.

doi:10.1128/AEM.02339-12

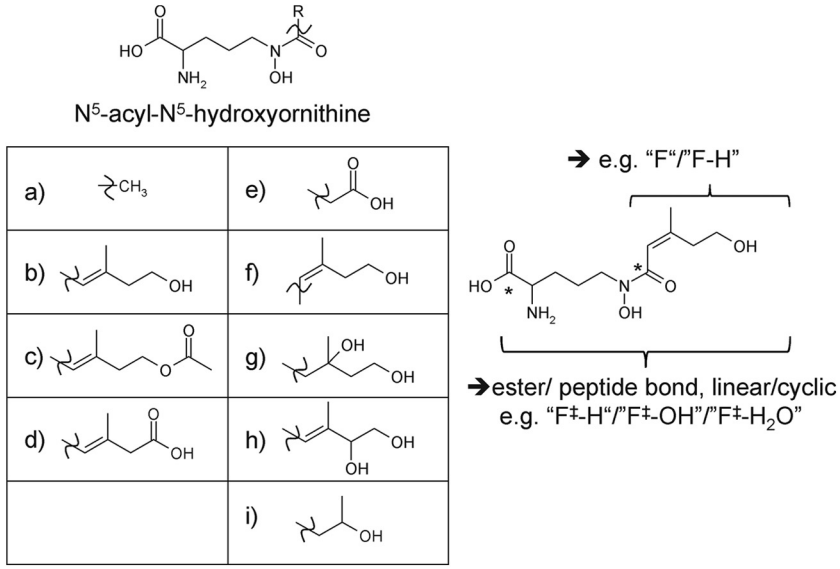

FIG 1 N^5-Acyl-N^5-hydroxyornithine units observed for known fungal siderophores; R can be any of the known residues shown in diagrams a to i (10). An example structure (by adding the moiety f to the N^5-hydroxyornithine unit) is shown on the right. The asterisk indicates the polar acyl or ester/peptide bond, the cleavage of which results in either the moiety shown in capital letters or the moiety shown in capital letters and "‡." The cleavage of these moieties results in characteristic siderophore fragments found in tandem mass spectrometry (see Table S2 in the supplemental material).

as agents of biological control of plant-pathogenic fungi (biocontrol) and are known siderophore producers (11). It has been shown that competition for iron plays a key role in the biocontrol exerted by *Trichoderma asperellum* strain T34 against *Fusarium oxysporum* f. sp. *lycopersici* (12). Dutta et al. (4) found that *Botrydiplodia theobromae* and *Fusarium* spp. produced only small amounts of siderophores compared to *Trichoderma* spp., indicating a more efficient way for *Trichoderma* to access the available iron. However, our knowledge on the diversity of siderophores produced by the different *Trichoderma* species is slight. Anke et al. (13) investigated the siderophore production of nine morphologically defined *Trichoderma* strains and detected the siderophores coprogen, coprogen B, ferricrocin, and fusigen type in the culture broths and coprogen, ferricrocin, and palmitoylcoprogen from the mycelia. Other studies additionally reported on the occurrence of *cis*- and *trans*-fusarinine, dimerum acid, ferrichrome C, fusarinine B, fusigen (fusarinine C), and N^{α}-dimethylisoneocoprogen II in various *Trichoderma* spp. (2, 14, 15).

Recent developments in mass spectrometry (MS) instrumentation give rise to new possibilities for the analysis of small molecules (e.g., metabolites present in biological samples) and exhibit both high mass resolution and good sensitivity. The acquisition of high-resolution full-scan mass spectral data allows for novel screening strategies by retrospective data analysis (16). Therefore, it can lead to novel insights into both the metabolic inventory of living systems and the underlying biological processes. These approaches are most powerful when combined with comprehensive database queries (17). Also, the diversity of *Trichoderma* species is well understood (reference 18 and references therein), and the genome sequences of three species (*T. atroviride*, *T. reesei*, and *T. virens*) are available (19, 20), enabling the interpretation of metabolites on the basis of the genes present.

In this study, liquid chromatography coupled with high-resolution mass spectrometry (LC-HRMS) was used to screen automatically for iron chelators/siderophores. The established method was applied to culture broths of 10 different *Trichoderma* strains belonging to eight phylogenetic species in order to evaluate siderophore production. Moreover, interpretation of siderophore diversity and its relationship to the genetic inventory (NRPS genes) and taxonomy has been carried out for the first time.

MATERIALS AND METHODS

In-house siderophore library and tandem-MS (MS/MS) neutral-loss list of fungal siderophores. An in-house library of published siderophores was established. Therefore, elemental formulas and the most common ion species observed in electrospray ionization (ESI)-MS (protonated molecule, ammonium and sodium adduct) were calculated. The structures of many siderophores are available at Siderophore Base (http://bertrandsamuel.free.fr/siderophore_base/siderophores.php) and in an excellent review article by Hider and Kong (6).

To facilitate the interpretation of MS/MS spectra, common fragments of siderophore MS/MS spectra were collected from the literature, measurements of standard compounds, and theoretical considerations. Mass increments between two typical fragments in the MS/MS spectrum correspond to characteristic structural units of the intact siderophores (neutral losses [Fig. 1]) and were collected to form an MS/MS neutral-loss list.

Strains and reagents. The species and strains used in this study were selected based on their known mycoparasitic activity (I. S. Druzhinina and L. Espino de Ramer, unpublished data) (Table 1). We used the strongly opportunistic species *Hypocrea atroviridis*/*T. atroviride*, *T. asperellum*, *T. gamsii*, and *T. hamatum* from the section *Trichoderma*; *Hypocrea virens*/*T. virens*, *T. harzianum*, and the weak antagonist *T. pachybasioides*/*T. polysporum* from the section *Pachybasium*; and the moderate mycoparasite *H. jecorina*/*T. reesei* strain QM6a from the section *Longibrachiatum*. The strains are maintained at the Collection of Industrially Important Microorganisms (TUCIM) at Vienna University of Technology, Vienna, Austria. The origins of the respective strains and the GenBank accession numbers for their DNA barcodes are listed in Table 1.

Methanol (MeOH) (LiChrosolv; LC gradient grade), iron standard solution [1 g/liter Fe, $Fe(NO_3)_3$ in 0.5 mol/l HNO_3], $Mg(NO_3)_2 \cdot 6H_2O$, $MnSO_4 \cdot 4H_2O$, and $CaCl_2 \cdot 2H_2O$ were purchased from Merck (Darmstadt, Germany); acetonitrile (ACN) (HiPerSolv Chromanorm; high-performance liquid chromatography [HPLC] gradient grade), Tween 80, and

TABLE 1 Strains used in the study

Taxon	Code	TUCIM no.	Other collection code(s)	Origin	Ecology	Distribution	Mycoparasitic activity	DNA barcode marker
Section *Trichoderma*								
Hypocrea atroviridis/*Trichoderma atroviride*	at1680	1680	IMI 206040	Slovenia	Soil, dead wood	Cosmopolitan in temperate zones	Strong	http://genome.jgi-psf.org/Triat2/Triat2.home.html
	at2108	2108		Hungary	Soil		Strong	ITS1 and -2 rRNA, TUCIM unpublished
	atP1	4241	P1		Hybrid strain	Strong	ITS1 and -2 rRNA, GU197852	
T. asperellum	asp	2128		Russia	Soil	Cosmopolitan	Strong	*tef1*[c], TUCIM unpublished
T. gamsii	gam	2323		Italy	Soil	Cosmopolitan	Strong	*tef1*, EF488129
T. hamatum	ham	2689		Ethiopia	Rhizosphere of *Coffea arabica*	Cosmopolitan	Strong	ITS1 and -2 rRNA, TUCIM unpublished
Section *Pachybasium*								
H. virens/*T. virens*	vir	3530	CBS 249.59, Gv29-8[a]	USA	Soil	Cosmopolitan	Strong	http://genome.jgi-psf.org/TriviGv29_8_2/TriviGv29_8_2.home.html
H. pachybasioides/*T. polysporum*	poly	462		Australia	Bark	Cosmopolitan, rare	Weak[b]	ITS1 and -2 rRNA, AY240169
T. harzianum	harz	916	CBS 226.95[a]	UK	Soil	Cosmopolitan in temperate zones	Strong	*tef1*, AY605833
Section *Longibrachiatum*								
H. jecorina/*T. reesei*	rees	917	QM6a[a]	Solomon Islands	Military tents	Rare, tropical	Moderate	http://genome.jgi-psf.org/Trire2/Trire2.home.html

[a] Type strain for the species.
[b] I. S. Druzhinina and L. Espino de Rammer, unpublished data.
[c] *tef1*, translation elongation factor 1 alpha gene.

ethanol were purchased from VWR (Vienna, Austria); formic acid (FA) (MS grade), nitric acid TraceSelect (69%), chloramphenicol, $MgSO_4 \cdot 7H_2O$, $ZnSO_4 \cdot 7H_2O$, K_2HPO_4, KNO_3, L-asparagine, D-glucose, $CuSO_4 \cdot 5H_2O$, and reserpine were obtained from Sigma-Aldrich (Vienna, Austria). Ultrapure water (18.2 MΩcm) was prepared successively by reverse osmosis with an ELGA Purelab Ultra-AN-MK2 system (Veolia Water, Vienna, Austria) and used throughout the study. Nitric acid was diluted 1:200 with water (0.5% [vol/vol] HNO_3). Hydrochloric acid (HCl) (*pro analysi*; J. T. Baker) was purchased from Bartelt (Vienna, Austria).

Standards for siderophores (HPLC Calibration Kit Coprogens and Fusarinines and HPLC Calibration Kit Ferrichromes) were purchased from EMC (Tübingen, Germany).

Graphite furnace atomic absorption spectroscopy (GF-AAS). Fe determination of the cultivation medium was performed on a PerkinElmer 4100 ZL atomic absorption spectrometer equipped with a THGA graphite furnace and an AS-70 autosampler. Background correction was performed by longitudinal Zeeman effect. Platform atomization from a transversally heated pyrolytically coated graphite tube was applied. Argon was used as the purge gas, and $Mg(NO_3)_2$ (1.5 g/liter in 0.5% HNO_3 [vol/vol]) was used as the matrix modifier. Twenty microliters of sample and 10 μl modifier were injected (direct injection without further pretreatment). The temperature program consisted of 100°C for 6 s, 110°C for 30 s, 130°C for 45 s, 1,300°C for 30 s, 2,100°C for 4 s, and 2,400°C for 4 s. The working range was 5 μg/liter to 50 μg/liter Fe, and the limit of detection was estimated to be 2 μg/liter Fe by measuring blanks (0.5% [vol/vol] HNO_3) and low-Fe-matrix samples. Standard addition revealed no significant sensitivity change due to the matrix.

Cultivation conditions and sampling. All glassware was rinsed twice with 6 M HCl, followed by five times with ultrapure water prior to use in order to remove traces of iron.

The cultivation medium consisted of glucose (0.5% [mass/vol]), L-asparagine (0.5% [mass/vol]), K_2HPO_4 (0.08%[mass/vol]), KNO_3 (0.07% [mass/vol]), $MgSO_4 \cdot 7H_2O$ (0.05% [mass/vol]), $CaCl_2 \cdot 2H_2O$ (0.02% [mass/vol]), $MnSO_4 \cdot 4H_2O$ (0.001% [mass/vol]), $ZnSO_4 \cdot 7H_2O$ (0.001% [mass/vol]), and $CuSO_4 \cdot 5H_2O$ (0.0005% [mass/vol]). Chloramphenicol was prepared as a 30-mg/ml stock solution in 70% (vol/vol) ethanol and added to the liquid medium to a final concentration of 30 μg/ml to prevent bacterial contamination.

The fungal strains were pregrown on 2% (mass/vol) malt extract agar at 25°C with a 12-h light cycle. The inoculum was prepared after conidial maturation (2 to 3 days) by rolling a sterile, wetted cotton swab over conidiating areas. Conidia were suspended in sterile ultrapure water containing 0.03% (vol/vol) Tween 80 in disposable borosilicate test tubes. The concentration of the spore suspension was adjusted to a transmission of 0.31 using a Biolog turbidimeter (Biolog Inc., Hayward, CA) at an optical density at 590 nm (OD_{590}) corresponding to 6×10^6 conidia per ml. Then, 100 μl of the conidial suspension was dispensed into each well of 24-well plates (each well contained 2 ml of liquid medium). The microplates (Greiner, Germany) were incubated under controlled conditions (25°C; 12-h light/dark cycle). Mycelial growth was measured at OD_{750} after 24, 48, 72, and 96 h.

Culture broth from the wells was harvested after 48, 72, and 96 h and filtered through disposable syringe filters (0.45-μm cellulose; Asahi Glass Co., Ltd., Japan). Four technical replicates (inoculated from the same spore suspension) were taken for all strains. The three strains for which genome sequences are available (*T. atroviride* IMI 206040, *T. virens* Gv29-8, and *T. reesei* QM6a) were tested in three independent biological replicates.

Liquid chromatography–high-resolution (tandem) mass spectrometry analysis. To detect the ferriforms of the siderophores, 980 μl of filtered broth sample was mixed with 10 μl of aqueous $FeCl_3$ solution (2% [mass/vol] $FeCl_3$, 10% [vol/vol] FA) prior to LC-MS measurements.

Ten microliters and 20 μl of sample (full-scan MS and MS/MS measurements, respectively) were injected into the HPLC system (Accela; Thermo Fisher Scientific, San Jose, CA) equipped with a reversed-phase Atlantis dC_{18} analytical column, 150- by 2.1-mm inside diameter (i.d.), 3-μm particle size (Waters, Vienna, Austria), and a C_{18} 4- by 3-mm i.d. security cartridge (Phenomenex, Torrance, CA). The column temperature was maintained at 25°C. Eluent A was ultrapure water and eluent B was MeOH, both containing 0.1% (vol/vol) FA. For chromatographic separation, the initial mobile-phase composition (100% eluent A) was held constant for 1 min, followed by a linear gradient to 100% eluent B in

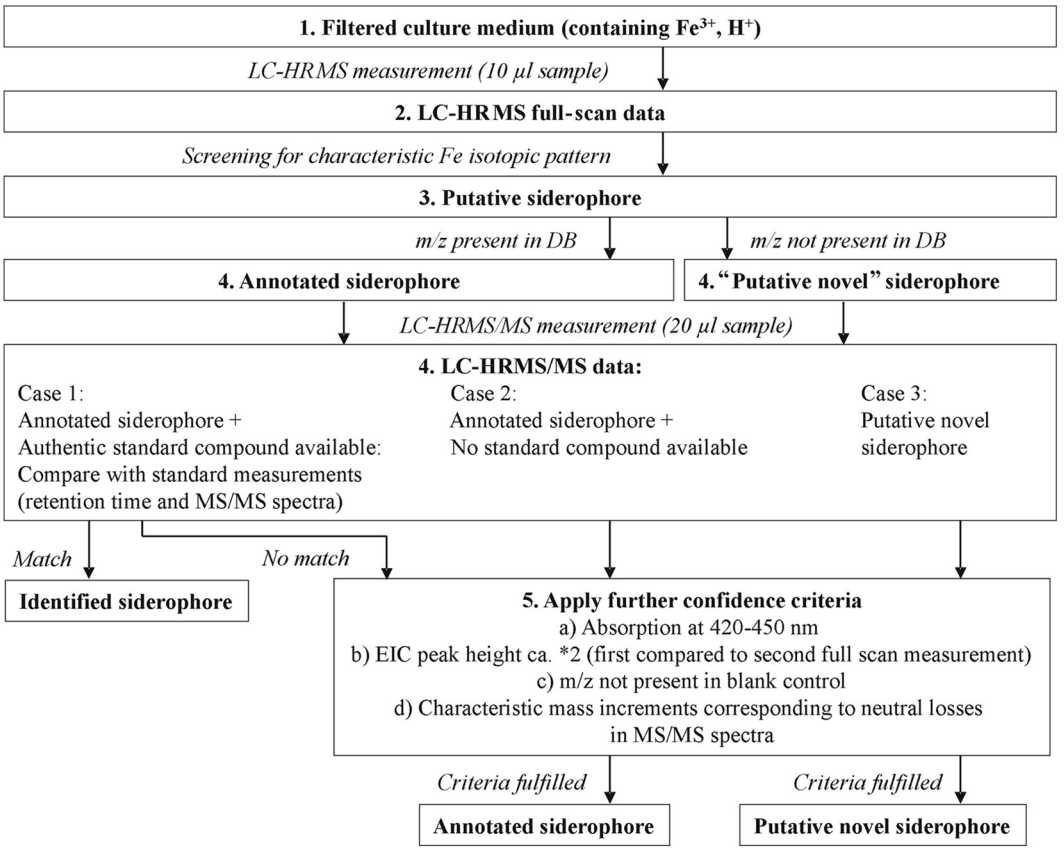

FIG 2 Work flow for the screening of siderophores by LC-HRMS(/MS).

35 min. This final condition was held for 4.5 min, followed by 4-min column reequilibration at 100% eluent A. The flow rate was 200 µl/min.

The HPLC system was coupled to an Accela PDA (scan wavelength, 200 to 600 nm; bandwidth, 1 nm; scan rate, 20 Hz) and subsequently to an LTQ Orbitrap XL (both Thermo Fisher Scientific) equipped with an ESI interface, which was operated in positive ionization mode using the following settings: electrospray voltage, 4 kV; sheath gas, 40 arbitrary units; auxiliary gas, 5 arbitrary units; capillary temperature, 300°C. All other source parameters were automatically tuned for a maximum MS signal intensity of reserpine solution. To this end, 10 µl/min of reserpine solution (10 mg/liter, dissolved in 8:2 [vol/vol] ACN-ultrapure water) was infused via syringe pump into the mobile phase (1:1 eluent A-eluent B) at a flow rate of 200 µl/min.

For the FT-Orbitrap full-scan and MS/MS measurements, the automatic gain control was set to a target value of 5×10^5, and a maximum injection time of 500 ms was chosen.

For the initial full-scan measurements, the mass spectrometer was used with a resolving power setting of 100,000 full width at half-maximum (FWHM) (at a mass-to-charge ratio [*m/z*] of 400) and a scan range of *m/z* 200 to 2,000. For subsequent MS/MS measurements, a survey full scan was followed by two data-dependent MS/MS measurements of the 1st and 2nd most intense ions from a parent mass list (obtained by initial screening of full-scan MS measurements at a parent mass width of 20 ppm and an isolation width of 2), all with a resolving power setting of 30,000 FWHM (at *m/z* 400). One MS/MS measurement was done using collision-induced dissociation (CID) (35% normalized collision energy), and another MS/MS measurement was done using higher-energy collision dissociation (HCD) (38% normalized collision energy). Data were generated using Xcalibur 2.1.0 (Thermo Fisher Scientific). Samples were measured in a randomized manner.

Evaluation of LC-MS(/MS) data. The analytical workflow is shown in Fig. 2. In the first step, raw data were automatically screened for the natural iron isotopic pattern in order to detect (putative novel) iron chelators. Therefore, the mass spectra were investigated; to be regarded as a possible iron chelator, a principal ion containing ^{56}Fe had to be accompanied by the corresponding ^{54}Fe isotopic signal at −1.99533 *m/z* with a maximum relative mass deviation of ±5 ppm (from the calculated mass of the ^{54}Fe signal) in the same spectrum. Also, the relative intensity of the ^{54}Fe-containing ion species had to be between 4 and 7% compared to the peak originating from the ^{56}Fe-containing ion. A minimum intensity of 10,000 counts was required for the monoisotopic ion.

The extracted ion chromatograms (EICs) of possible identified iron chelators (^{56}Fe- and ^{54}Fe-containing ion species) were extracted from raw data, and the Pearson's correlation coefficients of those EICs were calculated; as a threshold, a correlation coefficient of 0.75 had to be exceeded. To achieve peak annotation, the *m/z* values obtained were compared with the calculated *m/z* values of the protonated molecule, the ammonium and the sodium adduct of siderophores present in the in-house siderophore library (maximum relative mass deviation, ±5 ppm). In order to relate the peaks found to each other, for all putative iron chelators, the exact masses of ammonium and sodium adducts of each putative ion chelator were calculated and searched for in the spectra (maximum relative mass deviation, ±5 ppm). Additionally, manual curation and annotation of uncommon adducts and in-source fragments were performed.

For *m/z* values of iron chelators found via the screening approach, an Xcalibur processing method (Genesis peak detection algorithm) was generated to determine peak areas in the Xcalibur Quan Browser (Thermo Fisher Scientific). In this way, it was also possible to find some of the iron chelators in samples where the automated screening originally had failed to detect them (strict criteria).

The putative siderophore *m/z* values that were detected in all replicates were included in a parent mass list for further MS/MS investigation. If available, MS/MS spectra were compared with the MS/MS spectra of authentic standard compounds in order to identify known siderophores. If they were not available, further confidence criteria were applied to annotated siderophores (an *m/z* value was present in the in-house library, but no commercial standard was available) and "putative novel siderophores" (an *m/z* was not present in the in-house library). UV/visible (UV/Vis) chromatograms were evaluated at 420 to 450 nm, since most siderophores show absorption maxima between 420 nm and 450 nm (21). Between two full-scan measurements (first time, 10-μl injection volume; second time, 20-μl injection volume), the peak heights had to increase by approximately a factor of 2 in order to ensure that it was a reliable signal. Additionally, *m/z* values that also occurred in the blank control (culture medium plus ultrapure water, Tween 80, and aqueous $FeCl_3$ solution) were eliminated and not further considered. Finally, MS/MS spectra were searched for characteristic mass increments from the MS/MS neutral-loss list of fungal siderophores (see Table S2 in the supplemental material). First, the parent masses that were selected for further MS/MS investigation were tested if they exhibited the natural iron isotopic pattern. Base peaks of MS/MS spectra had to show a minimum intensity of 100 counts. Only fragment ions with a minimum relative intensity of 15% relative to the base peak were considered. For each fragment ion observed in an MS/MS spectrum, potential masses of related fragments were calculated based on the MS/MS neutral-loss list. The corresponding calculated *m/z* values were compared to the observed ions in a spectrum. To be correctly assigned, a maximum relative mass deviation of ±10 ppm had to be achieved.

Fungal siderophores mostly possess a mass of ≥500 Da. Therefore, iron chelators found with our screening approach exhibiting a molecular mass below 500 Da were excluded from this study, since they might be the result of degradation processes.

Genome-wide screening for siderophore synthetase genes in *Trichoderma*. The publicly available genome databases (JGI; http://genome.jgi-psf.org) for *T. atroviride*, *T. reesei*, and *T. virens* were screened for NRPS genes that might be involved in the biosynthesis of siderophores. A similarity search (BLASTP) of all NRPS protein sequences found in *Trichoderma* genomes (19) as queries against all available fungal genomes revealed 353 homolog NRPS protein sequences. The multiple-sequence alignment was assembled in ClustalX (22), and the maximum-parsimony phylograms were constructed as implemented in PAUP*4.0b10 (heuristic search with 1,000 replicates; Maxtrees in effect). The resulting tree was screened for annotated siderophore synthetases. All orthologous NRPSs that are putatively involved in siderophore biosynthesis, as well as other orthologous genes found in the literature that contribute to siderophore synthesis, were independently analyzed by similarity searchs (BLASTP) of their protein sequences in the NCBI database (http://blast.ncbi.nlm.nih.gov/Blast.cgi).

RESULTS

In-house siderophore library and MS/MS neutral-loss list of fungal siderophores. An in-house library of microbial siderophores was generated (as a Microsoft Excel spreadsheet), including siderophores described in the literature (6, 10, 23–40). The library contains the elemental formulas and theoretical masses of the protonated molecules and the ammonium and sodium adducts of ferriforms of published siderophores. In bi- and tetradentate iron chelators, the protonated molecule corresponds to the dimer $[Fe^{3+}SID_2\text{-}3H^+ + H]^+$ and in tetradentate and hexadentate chelators to $[Fe^{3+}SID\text{-}3H^+ + H]^+$. Currently, the in-house library consists of 422 entries of bacterial (ca. 90%) and fungal (ca. 10%) siderophores and is freely available on request from the laboratory of the corresponding author.

A list of *m/z* values originating from neutral losses caused by MS/MS fragmentation of known fungal siderophores was generated based on the literature (41–44) and MS/MS measurements of authentic siderophore standards (see Table S2 in the supplemental material). Additionally, the potential mass increments originating from neutral losses after rupture of the acyl bonds of N^5-acyl-N^5-hydroxyornithine units or the ester/peptide bonds between such building blocks (for known acyl groups a to i [10]) (Fig. 1) were added to the list of neutral losses. Not all of those neutral losses have been reported in the literature. Nevertheless, in analogy to earlier reports, fragmentation at these bonds can be expected due to the high polarity of the acyl bond (resulting in mass increments indicated as capital letters in Fig. 1). Moreover, the cleavage of an ester/peptide bond results in mass increments that are indicated as capital letters and "‡" in Fig. 1.

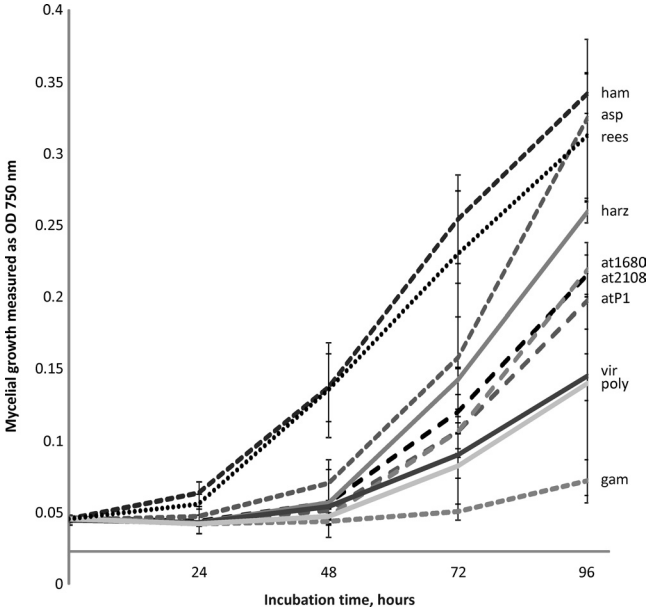

FIG 3 Growth of *Trichoderma* strains used in this study measured as mycelial density at OD_{750}. The strains were cultivated with supplementation by asparagine and zinc sulfate. The error bars show standard deviations; $n = 4$. ham, *T. hamatum*; asp, *T. asperellum*; rees, *T. reesei*; at1680, *T. atroviride* IMI 206040; at2108, *T. atroviride* TUCIM 2108; atP1, *T. atroviride* P1; harz, *T. harzianum*; poly, *T. polysporum*; gam, *T. gamsii*.

***Trichoderma* spp. are able to grow under conditions of Fe depletion.** We used a medium with neutral pH containing extra asparagine and zinc sulfate, because these conditions have been reported to be optimal for siderophore production (4, 13, 45). Chloramphenicol was added to the cultivation medium to prevent false-positive findings due to bacterial growth and thereby formation of bacterial siderophores. Prior to cultivation, growth media were measured by GF-AAS; the iron concentration was below 3 μg/liter Fe (corresponding to approximately 5×10^{-8} M Fe, conditions of iron depletion). Under these low-iron conditions, no significant differences were detected in growth when medium with or without iron or asparagine was used; however, siderophore production was increased by asparagine and zinc sulfate supplementation (data not shown). *Trichoderma* strains were in the exponential growth phase at all time points when the samples were taken (Fig. 3). No conidiation was observed during the experiment.

Interestingly, under the conditions of the experiment, the 10

strains showed different growth rates, with *T. hamatum*, *T. asperellum*, and *T. reesei* producing the highest biomass after 96 h. *T. gamsii*, which is a fast-growing fungus on complex media (46), had an extended lag phase up to 72 h and started to develop mycelial growth only close to the end of experiment. At the first sampling point (48 h), only *T. hamatum* and *T. reesei* had produced considerable biomass, while all other species had only begun to grow. However, nearly equal amounts and numbers of siderophores were detected at this time point for at least six tested strains: *T. hamatum*, *T. asperellum*, and *T*, *harzianum*, eight; *T. reesei*, *T. atroviride* IMI 206040, and *T. virens*, seven.

***Trichoderma* spp. produce a high diversity of extracellular iron chelators.** Figure 4 shows that in total, 18 siderophores were detected for the tested *Trichoderma* species when following the established workflow (Fig. 2). Examples of EIC and UV/Vis chromatograms are shown in Fig. S1 in the supplemental material. Based on absolute measured signal intensities in the supernatants, the highest concentration of most extracellular (putative) siderophores was observed after a cultivation duration of 96 h. Therefore, these supernatants were used for MS/MS measurements. Under the tested conditions, characteristic neutral losses for hydroxamate siderophores (see Table S2 in the supplemental material) were found in the MS/MS spectra (Table 2) of all Fe-containing metabolites. For identified siderophores, the *m/z* in Table 2 corresponds to the protonated molecules. In cases of annotated/putative novel siderophores, the protonated molecule was annotated based on the presence of the most common adduct ions (if present in the mass spectra).

The highest number of iron chelators, 15, was found for *T. harzianum*, followed by 14 in cultures of two strains of *T. atroviride* (IMI 206040 and P1). *T. gamsii* and *T. reesei* displayed the lowest number, with only 12 iron chelators detected, while all other strains/species exhibited 13 siderophores (Fig. 4). Dimerum acid, coprogren, and fusigen (identified) were produced by all *Trichoderma* strains; ferricrocin (identified) was produced by all *Trichoderma* strains but *T. gamsii* and *T. polysporum* and was detected at relatively low abundance compared to the other siderophores. Also, fusarinine A was produced by all strains (annotated), although it was significantly more abundant in *T. harzianum* and *T. reesei* than in all other strains. *T. reesei* was the only strain that produced *cis*-fusarinine (annotated), which occurred as both a monomer and a dimer, the latter being more abundant. The EIC at *m/z* 798.309 showed three distinct characteristic peaks at different retention times: 11.7 min (*T. reesei* and *T. harzianum*), 12.7 min, and 13.2 min (all strains but *T. reesei*). This mass signal corresponds to the protonated molecules of the known isomeric siderophores fusarinine B and des-diserylglycylferrirhodin (DDF). The MS/MS spectra of all three of these iron chelators exhibit characteristic mass increments for hydroxamate siderophores. Both, fusarinine B and DDF consist of the same structural subunits (three N^5-acyl-N^5-hydroxyornithine units with three "F" residues [Fig. 1]) and corresponding neutral losses ($\Delta m/z$, 242.127, corresponding to F‡-H_2O [see Table S2 in the supplemental material]) were found in the MS/MS spectra of all three compounds. The chromatographic peak at 11.7 min exhibited extensive in-source fragmentation. Nevertheless, unambiguous assignment of the three MS/MS spectra to the two known siderophores was not possible. Moreover, seven putative novel siderophores were produced by *T. atroviride* strains IMI 206040 and P1 (similar patterns) and *T. harzianum*; six by *T. asperellum*, *T. atroviride* TUCIM 2108, *T. gamsii*, *T. hamatum*, *T. polysporum*, and *T. virens* (similar patterns); and two by *T. reesei* (*m/z* 798.309 was not considered a novel siderophore). The most distinctive profile of siderophores was found in *T. reesei*, which produces one unique compound (*cis*-fusarinine) and three other iron-chelating metabolites present only in *T. harzianum* (Fig. 4). The siderophore production patterns of all other strains were relatively similar, with *T. harzianum* displaying the highest siderophore diversity. To see whether siderophore production and diversity correspond to the phylogeny of the genus, we constructed a cladogram, which shows the reasonable groupings within the genus (Fig. 4).

The three biological replicates of the sequenced *Trichoderma* strains revealed consistent qualitative siderophore profiles and only minor differences in relative siderophore abundances (see Table S1 in the supplemental material).

Although the three *T. atroviride* strains were isolated from different ecosystems and locations, they show similar siderophore production patterns. IMI 206040 and P1 produced 14 and TUCIM 2108 13 (putative) siderophores. They produced the same siderophores, the only exception being *m/z* 902.333 (18.9 min), which was not found in TUCIM 2108 (Fig. 4). The signal with *m/z* 902.333 showed very low intensity, which might explain why it was not found in the other strain.

Siderophore production in relation to genomic inventory. In order to understand the diversity of *Trichoderma* siderophores found in this study, we performed a phylogenetic analysis of all NRPS protein sequences found in the genomes of *T. atroviride*, *T. reesei*, and *T. virens*, as well as all their fungal orthologues obtained from the JGI genome database. Furthermore, we screened the literature for genes involved in siderophore production in other fungal genera and searched for homologs in *Trichoderma* genomes (Table 3).

Our phylogenetic analysis resulted in three clades containing orthologous genes related to siderophore biosynthesis (data not shown). (i) *T. atroviride* (gene ID 318290), *T. reesei* (gene ID 69946), and *T. virens* (gene ID 85582) orthologues coding for putative protein-containing domains consistent with *A. fumigatus* SidA (JGI genome annotation of *T. reesei*, gene ID 69946 [http://genome.jgi-psf.org]); (ii) *T. reesei* and *T. virens* orthologues (gene ID 71005 and 70206, respectively) related to nonribosomal peptide synthetase SidD in *A. fumigatus and A. clavatus*; (iii) a *Trichoderma* homolog of nonribosomal peptide synthetase, related to NPS6 (siderophore) of *Cochliobolus heterostrophus* (*T. atroviride*, *T. reesei*, and *T. virens*; gene ID 44273, 67189, and 39887, respectively), putatively involved in fusarinine synthesis in *Aspergillus nidulans*, *Aspergillus oryzae*, and *Fusarium graminearum* (47, 48). Furthermore, homologs of *sidL* and *sidC* genes involved in *A. fumigatus* biosynthesis of ferricrocin (49) and all homologs of *sidI*, *sidH*, and *sidF* genes, together with orthologues *NPS6* and *sidD* stepwise involved in the biosynthesis of fusarinine C (49–51), were found in all three *Trichoderma* spp. (Table 3). However, the homolog of acetyltransferase SidG (51), which is required for conversion of fusarinine C (fusigen) into triacetylfusarinine C in *A. fumigatus*, was found only in *T. virens*.

DISCUSSION

In this study, we established an LC-HRMS/MS screening approach to study the production of extracellular iron-containing metabolites in microbial samples.

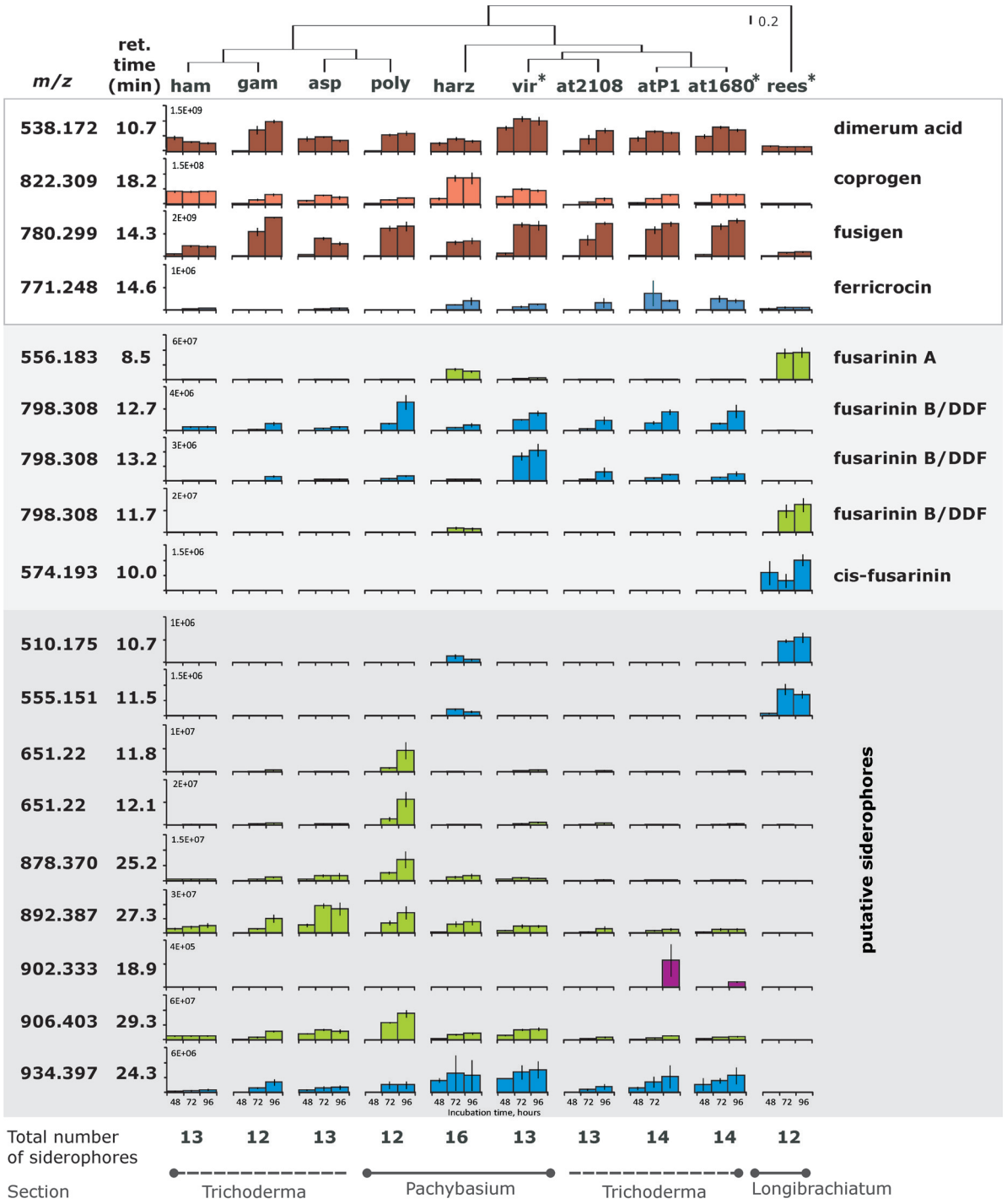

FIG 4 Siderophore production in *Trichoderma* species detected using full-scan and MS/MS measurements (signal intensities were normalized to mycelial production): *T. atroviride* (at2108, at1680, and atP1 for TUCIM 2108, IMI 206040, and P1, respectively), *T. hamatum* (ham), *T. virens* (vir), *T. harzianum* (harz), *T. polysporum* (poly), *T. asperellum* (asp), *T. gamsii* (gam), and *T. reesei* (rees). Dimerum acid, coprogen, fusigen, and ferricrocin were identified; fusarinine A, fusarinine B/DDF, and *cis*-fusarinine were annotated (no unambiguous annotation of fusarinine B/DDF was possible). The strains with sequenced genomes are marked with asterisks. The different colors represent different concentration ranges. The vertical cladogram was obtained based on a complete linkage rule using 1− Pearson's *R* distance. The vertical lines indicate standard deviations; $n = 4$.

To facilitate the analysis of siderophores in microbial cultures, an in-house siderophore library was established containing 422 entries for bacterial (ca. 90%) and fungal (ca. 10%) siderophores. Fungal siderophores show higher structural similarity than bacterial siderophores, which allowed the generation of an MS/MS neutral-loss list of fungal siderophores. Subsequently, a novel screening method for siderophores was established using LC-HRMS/MS. The screening approach was applied to investigate the

TABLE 2 Characteristic neutral losses of MS/MS spectra found for observed (putative novel) siderophores[r]

Name (annotated)	*m/z* (retention time [min])	Elemental formula(s) corresponding to experimentally determined neutral losses in spectra[n]	
		CID	HCD
Fusarinine A	556.183[p] (8.5)	$C_6H_8O_2$[a,b,c], $C_6H_{10}O_3$[c]	C_4H_4[d], C_5H_6[d], $C_6H_8O_2$[a,b,c], $C_{11}H_{19}N_2O_5$[e]
cis-Fusarinine (dimer)	574.193[q] (10.0)	$C_6H_8O_2$[a,b,c], $C_6H_{10}O_3$[c] (2×)	$C_3H_5NO_3$[d], $C_5H_{10}N_2O_2$[a], $C_5H_8N_4O_3$[f], $C_{11}H_{19}N_2O_5$[e], $C_{11}H_{20}N_2O_5$[e], $C_{11}H_{21}N_2O_6$[e]
Fusarinine B/DDF[o]	798.309[q] (11.7)	$C_6H_8O_2$[a,b,c] (3×), $C_6H_{10}O_3$[c], $C_5H_{10}N_2O_2$[a], $C_{11}H_{18}N_2O_4$[g], $C_{11}H_{20}N_2O_5$[e] (2×)	
Fusarinine B/DDF[o]	798.309[q] (12.7)	C_4H_4[d] (2×), $C_6H_{10}O_3$[c], $C_5H_{10}N_2O_2$[a], $C_7H_{12}N_2O_3$[a,g] (2x), $C_{11}H_{18}N_2O_4$[g] (3×), $C_{11}H_{20}N_2O_5$[e]	$C_6H_8O_2$[a,b,c], $C_7H_{12}N_2O_3$[a,g], $C_{11}H_{18}N_2O_4$[g], $C_{11}H_{20}N_2O_5$[e], $C_{13}H_{20}N_2O_5$[a,e,h]
Fusarinine B/DDF[o]	798.309[q] (13.2)	C_4H_4[d], $C_6H_{10}O_3$[c], $C_{11}H_{18}N_2O_4$[g], $C_{11}H_{20}N_2O_5$[e]	C_2H_2O[c,i], $C_9H_{16}N_2O_4$[e]
Unknown	510.175[p] (10.7)	$C_6H_8O_2$[a,b,c] (2×), $C_{12}H_{19}NO_4$[b]	$C_{11}H_{17}N_2O_5$[e], $C_{11}H_{19}N_2O_5$[e]
Unknown	555.151[p] (11.5)	$C_6H_8O_2$[a,b,c]	C_5H_6[d]
Unknown	651.220[p] (11.8)	C_2H_4O[b], C_4H_4[d], C_3H_5O[i], C_5H_6[d], $C_6H_8O_2$[a,b,c] (2×), $C_4H_7NO_3$[d], $C_5H_{10}N_2O_2$[a], $C_5H_9NO_3$[j], $C_9H_{17}N_2O_3$[j,k] (2×), $C_8H_{12}N_2O_5$[e], $C_9H_{17}N_2O_4$[e], $C_{11}H_{17}N_2O_4$[e], $C_{11}H_{18}N_2O_4$[g] (2×), $C_{11}H_{16}N_2O_5$[e], $C_{11}H_{17}N_2O_5$[e] (2×), $C_{11}H_{18}N_2O_5$[e], $C_{11}H_{19}N_2O_5$[e] (3×), $C_{11}H_{20}N_2O_5$[e] (2×), $C_{11}H_{21}N_2O_5$[e] (2×), $C_{11}H_{17}N_2O_6$[e], $C_{11}H_{19}N_2O_6$[e], $C_{11}H_{21}N_2O_6$[e]	
Unknown	651.220[p] (12.1)	C_2H_2O[c,i] (2×), C_4H_4[d], C_5H_6[d] (2×), $C_6H_8O_2$[a,b,c] (2×), $C_6H_{11}N_2O_4$[a,l], $C_9H_{17}N_2O_3$[j,k] (2×), $C_{11}H_{17}N_2O_4$[e] (2×), $C_{11}H_{18}N_2O_4$[g] (2×), $C_{11}H_{19}N_2O_4$[e] (2×), $C_{11}H_{16}N_2O_5$[e], $C_{11}H_{17}N_2O_5$[e] (2×), $C_{11}H_{18}N_2O_5$[e] (2×), $C_{11}H_{19}N_2O_5$[e] (3×), $C_{11}H_{20}N_2O_5$[e] (2×), $C_{11}H_{21}N_2O_5$[e], $C_{11}H_{19}N_2O_6$[e], $C_{11}H_{21}N_2O_6$[e]	
Unknown	878.370[q] (25.2)	$C_6H_8O_2$[a,b,c], $C_6H_9O_3$[c], $C_6H_{10}O_3$[c] (4×), $C_{12}H_{19}NO_4$[b]	C_5H_6[d], $C_6H_8O_2$[a,b,c], $C_6H_{10}O_3$[c]
Unknown	892.387[q] (27.3)	$C_6H_8O_2$[a,b,c] (2×), $C_6H_8O_3$[c], $C_6H_{10}O_3$[c] (3×), $C_{12}H_{19}NO_4$[b]	C_2H_4O[b], C_4H_4[d], C_5H_6[d] (2×), $C_6H_8O_2$[a,b,c] (3×), $C_6H_8O_3$[c], $C_7H_{16}N_2O_2$[k]
Unknown	902.333[q] (18.9)	C_3H_5O[i], $C_4H_7O_2$[c], $C_6H_8O_2$[a,b,c], $C_{11}H_{18}N_2O_4$[g], $C_9H_{16}N_2O_4$[e], $C_5H_{12}N_2O$[l], $C_5H_{10}N_2O_2$[a]	
Unknown	906.403[q] (29.3)	$C_6H_8O_2$[a,b,c], $C_6H_{10}O_3$[c] (3×), $C_{12}H_{19}NO_4$[b]	
Unknown	934.397[q] (24.3)	$C_6H_8O_2$[a,b,c], $C_5H_{14}N_2O$[k], $C_6H_{10}O_3$[c] (4×), $C_8H_{16}O_3$[m], $C_8H_{13}N_2O_5$[e], $C_9H_{17}N_2O_4$[e], $C_9H_{17}N_2O_5$[e], $C_{12}H_{19}NO_4$[b]	C_4H_4[d], C_5H_6[d], $C_6H_8O_2$[a,b,c], $C_6H_{11}O_3$[c]

[a] Reported for fusarinines (20).
[b] Reported for coprogens (20).
[c] Expected/typical for acyl loss (e.g., F-H).
[d] Reported for cyclic ferrioxamines (20).
[e] Expected, typical for loss of N^5-acyl-N^5-hydroxyornithine unit (e.g., F‡-H).
[f] Reported for ferrichromes (41).
[g] Reported for ferrichromes (20).
[h] Observed for MS/MS measurement of triacetylfusigen standard.
[i] Reported for Fe-rhodotoluate (20).
[j] Expected, in analogy to observed neutral losses (20).
[k] Reported for desferrioxamine B (42).
[l] Observed for MS/MS measurement of fusigen standard.
[m] Reported for dimerum acid (44) and observed for MS/MS measurement of dimerum acid standard.
[n] 2×/3×, neutral loss two/three times that observable in the MS/MS spectrum.
[o] Unambiguous annotation not possible.
[p] Ion species not identified.
[q] Protonated molecule.
[r] Siderophores for which standards were available are not included.

production of extracellular siderophores of 10 wild-type *Trichoderma* strains attributed to eight species covering the three major sections of the genus. A number of strict screening criteria were defined in order to ensure that compounds were indeed iron chelators produced by the fungi under investigation. They included verification of low-iron conditions by GF-AAS, addition of chloramphenicol to the culture medium in order to exclude bacterial contamination (production of bacterial siderophores), a realistic mass range allowing putative novel siderophores known from former publications, a characteristic iron isotopic pattern

TABLE 3 Identified and annotated siderophores detected in this study and the genes putatively involved in their synthesis

Siderophore name (*m/z*; retention time [min])	Type	*Trichoderma* genes involved in siderophore biosynthesis								
			T. virens		*T. atroviride*		*T. reesei*			
		Gene name(s)	GenBank no.	E value[b]	GenBank no.	E value	GenBank no.	E value	Annotation	Reference(s)
All	All	*sidA*	EHK26838	2E−162	EHK44669	2E−144	EGR44632	1E−161	The initial biosynthetic step, shared by pathways of both intra- and extracellular siderophore biosynthesis, is catalyzed by the ornithine-N^5-monooxygenase SidA (in *A. fumigatus* XP_755103).	50
Ferricrocin (771.248; 14.6)	Ferichrome	*sidL*	EHK18514	5E−145	EHK46975	2E−144	EGR46972	9E−135	Biosynthesis of ferricrocin and hydroxyferricrocin involves acetylation of N^5-hydroxyornithine to N^5-acetyl-N^5-hydroxyornithine by SidL in *A. fumigatus* (XP_750193).	49
		sidC, *sid2*, *NPS2*	EHK26839	0E+00	EHK44670	0E+00	EGR44663	0E+00	In *A. fumigatus*, NRPS SidC (XP_753088; Sid2 in *U. maydis*) couples 3 acetylhydroxyornithine molecules to 1 serine and 2 glycine residues to yield cyclic ferricrocin.	
Coprogen (822.309; 18.2) Fusigen (780.299; 14.3) *cis*-fusarin (574.193; 10.0) Fusarinine A[a] (556.183; 8.5) Fusarinine B[a] (798.309; 12.7)	Fusarinine/coprogen	*sidI*	EHK18683	0E+00	EHK45574	0E+00	EGR46098	0E+00	Acyl-CoA ligase SidI in *A. fumigatus* (XP_753087) converts mevalonate to mevalonyl-CoA.	51
		sidH	EHK21207, EHK20720, EHK20161	2E−102, 3E−89, 8E−85	EHK46085	3E-87	EGR44125, EGR44857, EGR49665	4E−98, 2E−91, 3E−84	Enoyl-CoA hydratase SidH in *A. fumigatus* (XP_748661) converts mevalonyl-CoA to anhydromevalonyl-CoA.	51
Dimerum acid (538.172; 10.7)		*sidF*	EHK21208	0E+00	EHK45575	3E−129	EGR44134	0E+00	In *A. fumigatus*, anhydromevalonyl-CoA is transferred to N^5-hydroxyornithine by the transacylase SidF (XP_748660) that is required for biosynthesis of fusarinine C and triacetylfusarinine C.	50
		NPS6	EHK18682	0E+00	EHK46196	0E+00	EGR46022	0E+00	NRPS related to NPS6 siderophore of *Cochliobolus heterostrophus* (AAX09988); NPS6 might produce a siderophore corresponding to fusarinine of *A. nidulans*, *A. oryzae*, and *F. graminearum* and coprogen in *Neurospora crassa* based on the domain structure of the predicted protein and sequence homology.	48[c]

sidD	ID 70206/EHK21211	0E+00		ID 71005/EGR44132	0E+00	Siderophore synthetase SidD, homologous to NPS6 of *Trichoderma* sp. NRPS SidD in *A. fumigatus* (XP_748662), transfers N^5-*cis*-anhydromevalonyl-N^5-hydroxy-L-ornithine to fusarinine C.	50[c]
sidG	EHK22271	2E−62				Acetyltransferase SidG is required for conversion of fusigen (fusarinine C) into triacetylfusarinine C in *A. fumigatus* (XP_748685).	50, 51

[a] Unambiguous annotation not possible.
[b] E values refer to the query accession number listed in annotation.
[c] Also *Trichoderma* genome annotation (http://genome.jgi-psf.org/pages/home.jsf?query=Trichoderma&searchType=Keyword).

present in the full-scan mass spectra, characteristic UV/Vis absorption of ferrisiderophores at 420 to 450 nm, increasing peak heights of putative novel siderophores in different measurements due to increased sample injection, measurement of a blank control to exclude false positives, and characteristic mass increments corresponding to neutral losses in MS/MS spectra of putative novel siderophores (Fig. 1).

Minor differences between the three biological replicates of the sequenced *Trichoderma* strains occurred and are explicable due to the already low intensity values (peak area, ca. 10^4 counts · s) in the replicates where they were found; their absence in the other replicates is most likely due to concentration variations (see Table S1 in the supplemental material). Three iron chelators were found in two of three biological replicates in *T. reesei*; they were removed only from the *T. reesei* results (Fig. 4 and Table 2), since they were consistently found in *T. atroviride* IMI 206040 and *T. virens*.

The putative siderophore with *m/z* 1121.344 was consistently found in all *Trichoderma* samples. Since it showed perfect coelution with dimerum acid, it was excluded from the results because it was likely being generated during the ionization process in the ESI ion source.

The screening approach applied suggested high diversity in siderophore production by *Trichoderma* spp. In total, 18 different siderophores were detected in the culture filtrates. Ferricrocin plays an important role in intracellular iron storage (52) and is usually described as an intracellular siderophore. Nevertheless, it has been previously reported to be found as a minor component in *Trichoderma* culture filtrates (13). Possibly, small amounts of ferricrocin are washed out from the mycelium during filtration of the culture broths. Dimerum acid has so far been described only for *T. virens* (15). The possibility that its presence, as well as the presence of fusarinine A, in all samples is due to hydrolysis of larger siderophores cannot be ruled out, since they constitute subunits of many other, larger siderophores. In total, at least 10 putative novel siderophores were found using our screening approach.

Our findings demonstrate the potential of LC-HRMS(/MS) screening methods using selected criteria for the elucidation of (putative novel) metabolites of special interest, e.g., siderophores, relevant to the molecular mechanisms regarding their beneficial use, e.g., their use as biocontrol agents.

Examples of the characterization of novel siderophores. The putative siderophore with *m/z* 878.371 was produced by all *Trichoderma* strains but *T. reesei* (Fig. 4). Figure 5 shows the EIC, the MS spectrum, and the MS/MS spectrum of *m/z* 878.371. Investigation of the MS/MS spectra revealed the mass increment between two signals in the MS/MS spectrum corresponding to the neutral losses (calculated values) Δ130.063, which is typical for the loss of $C_6H_{10}O_3$ caused by cleavage of the acyl bond of the N^5-acyl-N^5-hydroxyornithine unit (corresponding to "G-H" in Fig. 1 and Table S2 in the supplemental material); Δ112.052, indicating a loss of $C_6H_8O_2$ caused by either the rupture of the acyl bond of the N^5-acyl-N^5-hydroxyornithine unit (corresponding to "B-H"/"F-H" in Fig. 1 and in Table S2 in the supplemental material), but also described by Mawji et al. (43) for fusarinines and coprogens; and Δ241.131 ($C_{12}H_{19}NO_4$), described by Mawji et al. (43) for coprogens. Interestingly, there were two more similar (putative) siderophores that eluted one after another with a mass difference of ca. Δ14.016 (CH_2), namely, *m/z* 892.387 and 906.403 (also present in all *Trichoderma* strains but *T. reesei*), and showing similar characteristic mass increments in the MS/MS spectra that might

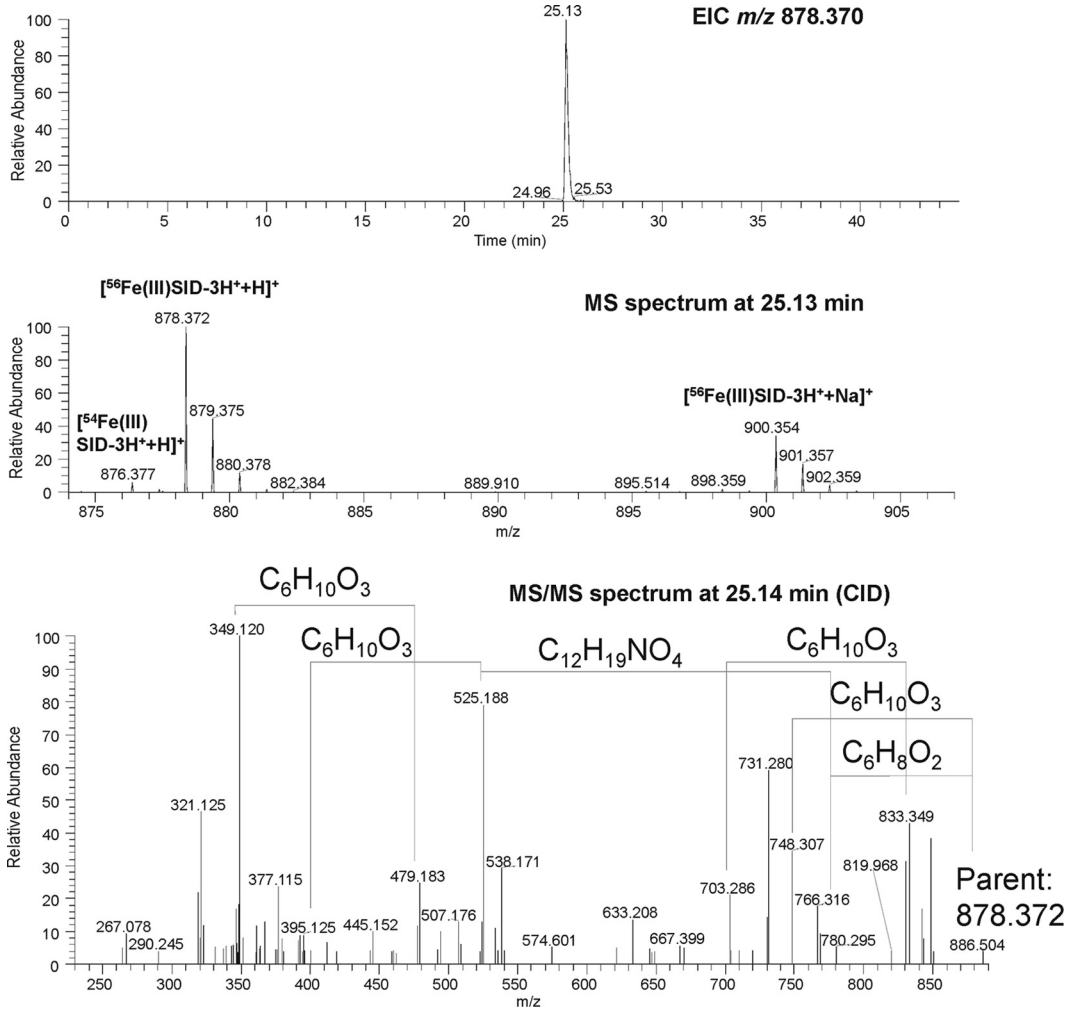

FIG 5 EIC of *m/z* 878.370 (±5 ppm), MS spectrum at a retention time of 25.13 min, and MS/MS spectrum (using CID) of *m/z* 878.372 at 25.14 min in *T. polysporum*. Elemental formulas corresponding to characteristic neutral losses of siderophores are indicated in the MS/MS spectrum.

indicate that they correspond to a homologous siderophore differing in a single CH_2 group.

The diversity of siderophores corresponds to the ecology of *Trichoderma* species. In this study, we tested one relatively (in relation to the average for the genus [I. S. Druzhinina and L. Espino de Rammer, unpublished data]) weak mycoparasitic species (*T. polysporum*) and one moderate (*T. reesei*, [53]) and six strong antifungal agents. The results show that the diversity of siderophores is not reflected in the degree of antagonistic activity of *Trichoderma* spp., as *T. polysporum* and the strongly mycoparasitic *T. gamsii* both had 12 siderophores detected. However, comparison of the ecologies of the tested species suggests a habitat bias: *T. reesei*, the species with the most distinctive siderophore profile, is a rare tropical species that is known only from several specimens isolated from wood from low levels of tropical rain forests. Unlike all other *Trichoderma* species, *T. reesei* has never been isolated from soil. Moreover, the species has an outstanding capacity to secrete cellulose-degrading enzymes. All other species are powerful environmental opportunists that are cosmopolitan and frequently isolated from soil, the rhizosphere, dead wood, and other fungi. Analysis of opportunistic species related to *T. reesei* (e.g., *T. longibrachiatum*) will be necessary to verify this hypothesis.

Low diversity of genes coding for siderophore synthetases in *Trichoderma* might indicate post-synthetic modifications as a reason for high compound diversity. As in other filamentous ascomycetes, *Trichoderma* siderophores are mostly produced nonribosomally by large multifunctional peptide synthetases, which are organized into repetitive synthase units. Each of the repetitive synthase units has functions required to complete a different single amino acid elongation step in the synthesis of the peptide product (15). The siderophores of *Trichoderma* spp. belong to the fusigen, ferrichrome, and coprogen families (54), and their orthologous NRPS gene clusters involved in siderophore synthesis (SidD and NPS6) have been identified in *T. atroviride*, *T. reesei*, and *T. virens* (19, 54).

Our phylogenetic analyses identified three clades involved in siderophore biosynthesis in three *Trichoderma* species: a putative ornithine-N^5-monooxygenase, SidA; an NPS6 siderophore synthetase; and a putative nonribosomal peptide synthetase, SidD. The last two are orthologous enzymes, yet *T. atroviride* contains the SidD homolog, which is more closely related to NPS6 of *C. heterostrophus*, whereas the other two species share orthologues closely related to both SidD and NPS6.

The ornithine-N^5-monooxygenase SidA is known to catalyze the initial step in siderophore biosynthesis in both intra- and ex-

tracellular siderophores (50). Genetic analysis of orthologues of *sidA* from *A. nidulans* (45, 55) and *A. fumigatus* (56), *dffA* from *A. oryzae* (57), and *sid1* from *F. graminearum* (58) revealed that the expression of the gene is repressed by iron, whereas gene disruption blocks the synthesis of all the hydroxamate siderophores each fungus can synthesize (49).

Numerous publications on *Aspergillus* spp. and other siderophore-producing fungi have reported several other genes that might be involved in siderophore production. Recently, it was reported that the biosynthesis of ferricrocin and hydroxyferricrocin involves acetylation of N^5-hydroxyornithine to N^5-acetyl-N^5-hydroxyornithine by the *sidL* gene (49). *sidL* was not found to be genomically clustered with other siderophore-biosynthetic genes, and it is not regulated by iron availability (49). We found that all three *Trichoderma* spp. possess a *sidL*-homologous gene that has 47 to 49% identity to *A. fumigatus*, with significant E values (Table 3).

Furthermore, Tobiasen et al. (47) recently reported that NPS2 encodes an NRPS with a composition analogous to the structure of SidC from *A. nidulans* (45) and Sid2 from *Ustilago maydis* (59), whose genes are known to produce the siderophores ferricrocin and ferrichrome, respectively. Schwecke et al. (60) concluded that NPS2 produces ferricrocin, based on the domain structure and architecture of the predicted enzyme. Additionally, it was shown that NPS2 in *F. graminearum* produces a siderophore corresponding to ferricrocin from *A. nidulans* (47). Corresponding to our detection of ferricrocin in *T. virens*, *T. atroviride*, and *T. reesei*, we found the highly similar orthologous genes *sidL* and *sidC* in the genomes of all three species (Table 3).

Moreover, it was recently shown that the biosynthesis of fusarinine- and coprogen-type siderophores in *A. fumigatus* requires five genes corresponding to *sidI*, *sidH*, *sidF*, *sidD*, and *sidF* (49–51), starting with the hydroxylation of ornithine, catalyzed by the monooxygenase SidA. Based on finding highly similar orthologues for all the genes involved in fusarinine C synthesis in *Trichoderma* spp. (Table 3), we propose that the production of fusarinine-type siderophores is similar to the well-understood process in *Aspergillus* spp. However, the nonribosomal siderophore synthetase SidD, which is involved in the last step of fusarinine C synthesis in *A. fumigatus* (51) (Table 3), or its orthologue NPS6 was present in all three *Trichoderma* spp., suggesting their important roles in fusarinine C production in *Trichoderma*.

We detected dimerum acid in all three *Trichoderma* spp., but until now, its production has been reported only for *T. virens* (15). Wilhite et al. (15) found that Psy1 disruptants produced normal amounts of gliotoxin in *T. virens* but grew poorly under low-iron conditions, suggesting that Psy1 plays a role in siderophore production. The disruptants could not produce the major *T. virens* siderophore dimerum acid, a dipetide of acylated N^5-hydroxyornithine (15). However, Wiest et al. (61) described Psy1 as a fragment of peptaibol synthase, which is unrelated to siderophore biosynthesis, and furthermore, stressed that it is unlikely that it is involved in dimerum acid biosynthesis because of the numerous dimerum acid/coprogen-type siderophore producers that lack Psy1 orthologues (61).

However, the diversity of siderophores excreted by *Trichoderma* spp. is much higher than the number of NRPS genes present in their genomes (Table 3). Nevertheless, the siderophore production pattern is not reflected in the phylogenetic diversity of NRPS siderophore synthetases. However, further biosynthetic modification of NRPS products by non-NRPS enzymes, such as transacetylases and oxygenases, has been reported (8). Our data suggest that the great diversity of siderophores found in this study might be the result of even more enzymes involved in the modification of siderophores. Modification by external enzymes (in *trans*-modifications) or enzymes that work postassembly could also support the diversity of siderophores found in our study (62). Such known modifications include glycosylation, halogenation, and oxidation/reduction.

Since the competition for iron can play a key role in the biological control exerted by *Trichoderma* spp., the new insights into the productivity and diversity of extracellular iron-containing metabolites that have been gained in our studies demonstrate the great value of the LC-HRMS/MS method developed for this research area.

ACKNOWLEDGMENTS

The Federal Country Lower Austria and the European Regional Development Fund (ERDF) of the European Union are acknowledged for financial support (grant number GZ WST3-T-95/001-2006) which also enabled the Ph.D. studies of Sylvia M. Lehner.

We thank Wolfgang Kandler for facilitation and support of the GF-AAS measurements. We are thankful to Christian P. Kubicek for the critical discussion of results. The assistance of Jasmin Dopplinger and Lukas Purgstaller in the establishment of the in-house siderophore library is gratefully acknowledged.

REFERENCES

1. **Riedel E.** 1994. Anorganische Chemie, 3rd ed. De Gruyter, Berlin, Germany.
2. **Renshaw JC, Robson GD, Trinci APJ, Wiebe MG, Livens FR, Collison D, Taylor RJ.** 2002. Fungal siderophores: structures, functions and applications. Mycol. Res. **106**:1123–1142.
3. **Haas H.** 2003. Molecular genetics of fungal siderophore biosynthesis and uptake: the role of siderophores in iron uptake and storage. Appl. Microbiol. Biotechnol. **62**:316–330.
4. **Dutta S, Kundu A, Chakraborty MR, Ojha S, Chakrabarti J, Chatterjee NC.** 2006. Production and optimization of Fe(III) specific ligand, the siderophore of soil inhabiting and wood rotting fungi as deterrent to plant pathogens. Acta Phytopathol. Entomol. Hung. **41**:237–248.
5. **Loper JE, Buyer JS.** 1991. Siderophores in microbial interactions on plant surfaces. Mol. Plant Microbe Interact. **4**:5–13.
6. **Hider RC, Kong XL.** 2010. Chemistry and biology of siderophores. Nat. Prod. Rep. **27**:637–657.
7. **Lemanceau P, Expert D, Gaymard F, Bakker PAHM, Briat JF.** 2009. Role of iron in plant-microbe interactions. Adv. Bot. Res. **51**:491–549.
8. **Haas H, Eisendle M, Turgeon BG.** 2008. Siderophores in fungal physiology and virulence. Annu. Rev. Phytopathol. **46**:149–187.
9. **Hördt W, Römheld V, Winkelmann G.** 2000. Fusarinines and dimerum acid, mono- and dihydroxamate siderophores from Penicillium chrysogenum, improve iron utilization by strategy I and strategy II plants. Biometals **13**:37–46.
10. **Jalal MAF, van der Helm D.** 1991. Isolation and spectroscopic identification of fungal siderophores. CRC Press, Boca Raton, FL.
11. **Benítez T, Rincón AM, Limón MC, Codón AC.** 2004. Biocontrol mechanisms of Trichoderma strains. Int. Microbiol. **7**:249–260.
12. **Segarra G, Casanova E, Aviles M, Trillas I.** 2010. Trichoderma asperellum strain T34 controls Fusarium wilt disease in tomato plants in soilless culture through competition for iron. Microb. Ecol. **59**:141–149.
13. **Anke H, Kinn J, Bergquist KE, Sterner O.** 1991. Production of siderophores by strains of the genus Trichoderma: isolation and characterization of the new lipophilic coprogen derivative, palmitoylcoprogen. Biol. Metals **4**:176–180.
14. **Jalal MA, Love SK, van der Helm D.** 1986. Siderophore mediated iron(III) uptake in Gliocladium virens. 1. Properties of cis-fusarinine, trans-fusarinine, dimerum acid, and their ferric complexes. J. Inorg. Biochem. **28**:417–430.
15. **Wilhite SE, Lumsden RD, Straney DC.** 2001. Peptide synthetase gene in Trichoderma virens. Appl. Environ. Microbiol. **67**:5055–5062.

16. **Krauss M, Singer H, Hollender J.** 2010. LC-high resolution MS in environmental analysis: from target screening to the identification of unknowns. Anal. Bioanal. Chem. **397**:943–951.
17. **Fiehn O, Barupal DK, Kind T.** 2011. Extending biochemical databases by metabolomic surveys. J. Biol. Chem. **286**:23637–23643.
18. **Druzhinina IS, Seidl-Seiboth V, Herrera-Estrella A, Horwitz BA, Kenerley CM, Monte E, Mukherjee PK, Zeilinger S, Grigoriev IV, Kubicek CP.** 2011. Trichoderma: the genomics of opportunistic success. Nat. Rev. Microbiol. **9**:749–759.
19. **Kubicek C, Herrera-Estrella A, Seidl-Seiboth V, Martinez D, Druzhinina I, Thon M, Zeilinger S, Casas-Flores S, Horwitz B, Mukherjee P, Mukherjee M, Kredics L, Alcaraz L, Aerts A, Antal Z, Atanasova L, Cervantes-Badillo M, Challacombe J, Chertkov O, McCluskey K, Coulpier F, Deshpande N, von Dohren H, Ebbole D, Esquivel-Naranjo E, Fekete E, Flipphi M, Glaser F, Gomez-Rodriguez E, Gruber S.** 2011. Comparative genome sequence analysis underscores mycoparasitism as the ancestral life style of Trichoderma. Genome Biol. **12**:R40.
20. **Martinez D, Berka RM, Henrissat B, Saloheimo M, Arvas M, Baker SE, Chapman J, Chertkov O, Coutinho PM, Cullen D, Danchin EGJ, Grigoriev IV, Harris P, Jackson M, Kubicek CP, Han CS, Ho I, Larrondo LF, de Leon AL, Magnuson JK, Merino S, Misra M, Nelson B, Putnam N, Robbertse B, Salamov AA, Schmoll M, Terry A, Thayer N, Westerholm-Parvinen A, Schoch CL, Yao J, Barabote R, Nelson MA, Detter C, Bruce D, Kuske CR, Xie G, Richardson P, Rokhsar DS, Lucas SM, Rubin EM, Dunn-Coleman N, Ward M, Brettin TS.** 2008. Genome sequencing and analysis of the biomass-degrading fungus Trichoderma reesei (syn. Hypocrea jecorina). Nat. Biotechnol. **26**:553–560.
21. **Konetschny-Rapp S, Huschka H-G, Winkelmanne G, Jung G.** 1988. High-performance liquid chromatography of siderophores from fungi. Biometals **1**:9–17.
22. **Thompson JD, Gibson TJ, Plewniak F, Jeanmougin F, Higgins DG.** 1997. The CLUSTAL X Windows interface: flexible strategies for multiple sequence alignment aided by quality analysis tools. Nucleic Acids Res. **25**:4876–4882.
23. **Barbeau K, Zhang G, Live DH, Butler A.** 2002. Petrobactin, a photoreactive siderophore produced by the oil-degrading marine bacterium Marinobacter hydrocarbonoclasticus. J. Am. Chem. Soc. **124**:378–379.
24. **Briskot G, Taraz K, Budzikiewicz H.** 1986. Pyoverdin-type siderophores from Pseudomonas aeruginosa. Z. Naturforsch. C **41**:497–506.
25. **Christ K, Al-Kaddah S, Wiedemann I, Rattay B, Sahl H-G, Bendas G.** 2008. Membrane lipids determine the antibiotic activity of the lantibiotic gallidermin. J. Membr. Biol. **226**:9–16.
26. **Domagal-Goldman SD, Paul KW, Sparks DL, Kubicki JD.** 2009. Quantum chemical study of the Fe(III)-desferrioxamine B siderophore complex: electronic structure, vibrational frequencies, and equilibrium Fe-isotope fractionation. Geochim. Cosmochim. Acta **73**:1–12.
27. **Drechsel H, Stephan H, Lotz R, Haag H, Zaehner H, Hantke K, Jung G.** 1995. Structure elucidation of yersiniabactin, a siderophore from highly virulent Yersinia strains. Liebigs Ann. 1727–1733.
28. **Ehlert G, Taraz K, Budzikiewicz H.** 1994. Bacterial constituents. LIX. Serratiochelin, a new catecholate siderophore from Serratia marcescens. Z. Naturforsch. C **49**:11–17.
29. **Hickford SJH, Kuepper FC, Zhang G, Carrano CJ, Blunt JW, Butler A.** 2004. Petrobactin sulfonate, a new siderophore produced by the marine bacterium Marinobacter hydrocarbonoclasticus. J. Nat. Prod. **67**:1897–1899.
30. **Ikeda Y, Furumai T, Igarashi Y.** 2005. Nocardimicins G, H and I, siderophores with muscarinic M3 receptor binding inhibitory activity from Nocardia nova JCM 6044. J. Antibiot. **58**:566–572.
31. **Kazmi SA, Shorter AL, McArdle JV, Ashiq U, Jamal RA.** 2010. Studies on the redox characteristics of ferrioxamine E. Chem. Biodivers. **7**:656–665.
32. **Kodani S, Ohnishi-Kameyama M, Yoshida M, Ochi K.** 2011. A new siderophore isolated from Streptomyces sp. TM-34 with potent inhibitory activity against angiotensin-converting enzyme. Eur. J. Org. Chem. **2011**: 3191–3196.
33. **Laatsch H.** 2007. Antibase 2007: the natural product identifier. Wiley-VCH, Weinheim, Germany.
34. **Lu FX, Jeffrey AM.** 1993. Isolation, structural identification, and characterization of a mutagen from Fusarium moniliforme. Chem. Res. Toxicol. **6**:91–96.
35. **Michalke R, Taraz K, Budzikiewicz H.** 1996. Azoverdin. An isopyoverdin. Z. Naturforsch. C **51**:772–780.
36. **Reid RT, Live DH, Faulkner DJ, Butler A.** 1993. A siderophore from a marine bacterium with an exceptional ferric ion affinity constant. Nature **366**:455–458.
37. **Sandy M, Butler A.** 2009. Microbial iron acquisition: marine and terrestrial siderophores. Chem. Rev. **109**:4580–4595.
38. **Voss J, Taraz K, Budzikiewicz H.** 1999. Bacterial constituents. Part 80. A pyoverdin from the Antarctica strain 51W of Pseudomonas fluorescens. Z. Naturforsch. C **54**:156–162.
39. **Yoganathan S, Sit CS, Vederas JC.** 2011. Chemical synthesis and biological evaluation of gallidermin-siderophore conjugates. Org. Biomol. Chem. **9**:2133–2141.
40. **Zhu B, Jeffrey AM.** 1993. Fusarin C: isolation and identification of two microsomal metabolites. Chem. Res. Toxicol. **6**:97–101.
41. **Gledhill M.** 2001. Electrospray ionisation-mass spectrometry of hydroxamate siderophores. Analyst **126**:1359–1362.
42. **Groenewold GS, Van Stipdonk MJ, Gresham GL, Chien W, Bulleigh K, Howard A.** 2004. Collision-induced dissociation tandem mass spectrometry of desferrioxamine siderophore complexes from electrospray ionization of UO_2^{2+}, Fe^{3+} and Ca^{2+} solutions. J. Mass Spectrom. **39**:752–761.
43. **Mawji E, Gledhill M, Worsfold PJ, Achterberg EP.** 2008. Collision-induced dissociation of three groups of hydroxamate siderophores: ferrioxamines, ferrichromes and coprogens/fusigens. Rapid Commun. Mass Spectrom. **22**:2195–2202.
44. **Simionato AVC, de Souza GD, Rodrigues E, Glick J, Vouros P, Carrilho E.** 2006. Tandem mass spectrometry of coprogen and deferoxamine hydroxamic siderophores. Rapid Commun. Mass Spectrom. **20**:193–199.
45. **Eisendle M, Oberegger H, Buttinger R, Illmer P, Haas H.** 2004. Biosynthesis and uptake of siderophores is controlled by the PacC-mediated ambient-pH regulatory system in Aspergillus nidulans. Eukaryot. Cell **3**:561–563.
46. **Jaklitsch WM, Samuels GJ, Dodd SL, Lu BS, Druzhinina IS.** 2006. Hypocrea rufa/Trichoderma viride: a reassessment, and description of five closely related species with and without warted conidia. Stud. Mycol. **56**: 135–177.
47. **Tobiasen C, Aahman J, Ravnholt KS, Bjerrum MJ, Grell MN, Giese H.** 2007. Nonribosomal peptide synthetase (NPS) genes in Fusarium graminearum, F. culmorum and F. pseudograminearum and identification of NPS2 as the producer of ferricrocin. Curr. Genet. **51**:43–58.
48. **Varga J, Kocsubé S, Tóth B, and Mesterházy Á.** 2005. Nonribosomal peptide synthetase genes in the genome of Fusarium graminearum, causative agent of wheat head blight. Acta Biol. Hung. **56**:375–388.
49. **Blatzer M, Schrettl M, Sarg B, Lindner HH, Pfaller K, Haas H.** 2011. SidL, an Aspergillus fumigatus transacetylase involved in biosynthesis of the siderophores ferricrocin and hydroxyferricrocin. Appl. Environ. Microbiol. **77**:4959–4966.
50. **Schrettl M, Bignell E, Kragl C, Sabiha Y, Loss O, Eisendle M, Wallner A, Arst HN, Jr, Haynes K, Haas H.** 2007. Distinct roles for intra- and extracellular siderophores during Aspergillus fumigatus infection. PLoS Pathog. **3**:1195–1207.
51. **Yasmin S, Alcazar-Fuoli L, Gruñdlinger M, Puempel T, Cairns T, Blatzer M, Lopez JF, Grimalt JO, Bignell E, Haas H.** 2012. Mevalonate governs interdependency of ergosterol and siderophore biosyntheses in the fungal pathogen Aspergillus fumigatus. Proc. Natl. Acad. Sci. U. S. A. **109**:E497–E504.
52. **Eisendle M, Schrettl M, Kragl C, Müller D, Illmer P, Haas H.** 2006. The intracellular siderophore ferricrocin is involved in iron storage, oxidative-stress resistance, germination, and sexual development in Aspergillus nidulans. Eukaryot. Cell **5**:1596–1603.
53. **Druzhinina IS, Komoń-Zelazowska M, Atanasova L, Seidl V, Kubicek CP.** 2010. Evolution and ecophysiology of the industrial producer Hypocrea jecorina (anamorph Trichoderma reesei) and a new sympatric agamospecies related to it. PLoS One **5**:e9191. doi:10.1371/journal.pone.0009191.
54. **Mukherjee PK, Buensanteai N, Moran-Diez ME, Druzhinina IS, Kenerley CM.** 2012. Functional analysis of non-ribosomal peptide synthetases (NRPSs) in Trichoderma virens reveals a polyketide synthase (PKS)/NRPS hybrid enzyme involved in the induced systemic resistance response in maize. Microbiology **158**:155–165.
55. **Oberegger H, Schoeser M, Zadra I, Abt B, Haas H.** 2001. SREA is involved in regulation of siderophore biosynthesis, utilization and uptake in Aspergillus nidulans. Mol. Microbiol. **41**:1077–1089.
56. **Schrettl M, Bignell E, Kragl C, Joechl C, Rogers T, Arst HN, Jr, Haynes K, Haas H.** 2004. Siderophore biosynthesis but not reductive iron assim-

ilation is essential for Aspergillus fumigatus virulence. J. Exp. Med. **200**: 1213–1219.
57. **Yamada O, Nan SN, Akao T, Tominaga M, Watanabe H, Satoh T, Enei H, Akita O.** 2003. dffA gene from Aspergillus oryzae encodes L-ornithine N^5 oxygenase and is indispensable for deferriferrichrysin biosynthesis. J. Biosci. Bioeng. **95**:82–88.
58. **Greenshields DL, Liu G, Feng J, Selvaraj G, Wei Y.** 2007. The siderophore biosynthetic gene SID1, but not the ferroxidase gene FET3, is required for full Fusarium graminearum virulence. Mol. Plant Pathol. **8**:411–421.
59. **Yuan WM, Gentil GD, Budde AD, Leong SA.** 2001. Characterization of the Ustilago maydis sid2 gene, encoding a multidomain peptide synthetase in the ferrichrome biosynthetic gene cluster. J. Bacteriol. **183**:4040–4051.
60. **Schwecke T, Gottling K, Durek P, Duenas I, Kaufer NF, Zock-Emmenthal S, Staub E, Neuhof T, Dieckmann R, von Dohren H.** 2006. Nonribosomal peptide synthesis in Schizosaccharomyces pombe and the architectures of ferrichrome-type siderophore synthetases in fungi. Chembiochem **7**:612–622.
61. **Wiest A, Grzegorski D, Xu BW, Goulard C, Rebuffat S, Ebbole DJ, Bodo B, Kenerley C.** 2002. Identification of peptaibols from Trichoderma virens and cloning of a peptaibol synthetase. J. Biol. Chem. **277**:20862–20868.
62. **Walsh CT, Chen H, Keating TA, Hubbard BK, Losey HC, Luo L, Marshall CG, Miller DA, Patel HM.** 2001. Tailoring enzymes that modify nonribosomal peptides during and after chain elongation on NRPS assembly lines. Curr. Opin. Chem. Biol. **5**:525–534.